

Long-Term Forecasting using Higher-Order Tensor RNNs

Rose Yu

ROSE@CALTECH.EDU

Stephan Zheng

STEPHAN@CALTECH.EDU

Anima Anandkumar

ANIMA@CALTECH.EDU

Yisong Yue

YYUE@CALTECH.EDU

*Department of Computing and Mathematical Sciences
California Institute of Technology
Pasadena, CA 91125, USA*

Editor: Francis Bach, David Blei and Bernhard Schölkopf

Abstract

We present Higher-Order Tensor RNN (HOT-RNN), a novel family of neural sequence architectures for multivariate forecasting in environments with nonlinear dynamics. Long-term forecasting in such systems is highly challenging, since there exist long-term temporal dependencies, higher-order correlations and sensitivity to error propagation. Our proposed recurrent architecture addresses these issues by learning the nonlinear dynamics directly using higher-order moments and higher-order state transition functions. Furthermore, we decompose the higher-order structure using the tensor-train decomposition to reduce the number of parameters while preserving the model performance. We theoretically establish the approximation guarantees and the variance bound for HOT-RNN for general sequence inputs. We also demonstrate 5 ~ 12% improvements for long-term prediction over general RNN and LSTM architectures on a range of simulated environments with nonlinear dynamics, as well on real-world time series data.

Keywords: Time Series, Forecasting, Tensor, RNNs, Nonlinear Dynamics

1. Introduction

One of the central questions in science is forecasting: given the past history, how well can we predict the future? In many domains with complex multi-variate correlation structures and nonlinear dynamics, forecasting is highly challenging since the system has long-term temporal dependencies and higher-order dynamics. Examples of such systems abound in science and engineering, from biological neural network activity, fluid turbulence, to climate and traffic systems (see, e.g., Figure 1). Since current forecasting systems are unable to faithfully represent the higher-order dynamics, they have limited ability for accurate *long-term* forecasting.

Therefore, a fundamental challenge is accurately modeling nonlinear dynamics and obtaining stable long-term predictions, given a dataset of realizations of the dynamics. Here, the forecasting problem can be stated as follows: how can we efficiently learn a model that, given only a few initial states, can predict a sequence of future states over a long horizon of T time-steps accurately and reliably?

Common approaches to forecasting include classic linear time series models such as auto-regressive moving average (ARMA), state space models such as hidden Markov model (HMM), and deep neural networks. See a survey on time series forecasting by (Box et al., 2015) and the references therein. A recurrent neural network (RNN), as well as its memory-based extensions such as the LSTM, is a class of models that have achieved state of the art performance on sequence prediction tasks from demand forecasting (Flunkert et al., 2017) to speech recognition (Soltau et al., 2016) and video analysis (LeCun et al., 2015). But most of these methods focus on short-term predictions, and often fail to generalize to nonlinear dynamics and forecast over long time horizons.

In this work, we propose **HOT-RNN**, a model class that is more expressive and empirically generalizes better than standard RNNs, for the same model capacity. **HOT-RNN** explicitly models the 1) *higher-order dynamics*, by incorporating a longer history and higher-order state interactions of previous hidden states; and 2) using *tensor trains decomposition* that greatly reduces the number of model parameters, while mostly preserving the correlation structure of the full-rank model. We prove that **HOT-RNN** is exponentially more expressive than standard RNNs for functions that satisfy certain regularity conditions. Our contributions can be summarized as follows:

- We propose a novel family of RNNs **HOT-RNNs** to encode non-Markovian dynamics and higher-order state interactions. To address the memory issue, we propose a tensor-train decomposition that makes learning tractable.
- We provide theoretical guarantees for the expressiveness of **HOT-RNNs** for nonlinear dynamics, and characterize the target dynamics and its **HOT-RNN** representation. In contrast, no such theoretical results are known for standard recurrent networks.
- We show that **HOT-RNNs** can forecast more accurately for significantly longer time horizons compared to standard RNNs and LSTMs on simulated data and real-world environments with nonlinear dynamics.

2. Related Work

Time series forecasting Time series forecasting is at the core of many dynamics modeling tasks. In statistics, classic work such as the ARMA or ARIMA model (Box et al., 2015) model a stochastic process with assumptions of linear dynamics. In the control and dynamical system community, estimating dynamics models from measurement data is also known as *system identification* (Ljung, 2001). System identification often requires strong parametric assumptions which are often challenging to find from first principles. Moreover, finding (approximate) solutions of complex nonlinear differential equations demands high computational cost. In our work, we instead take a “mode-free” approach to learn a powerful approximate nonlinear dynamics model.

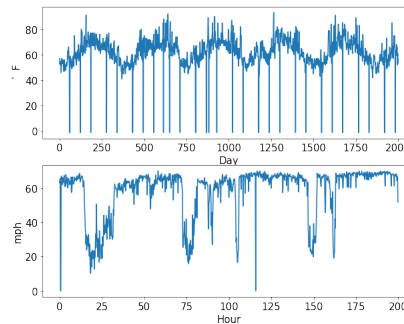


Figure 1: Climate and traffic time series visualization. The time series can be viewed as a realization of highly nonlinear dynamics.

Recurrent Neural Networks Using neural networks to model time series data has a long history (Schmidhuber, 2015). Recent developments in deep learning and RNNs has led to non-linear forecasting models such as deep AutoRegressive (Flunkert et al., 2017), Predictive State Representation (Downey et al., 2017), Deep State Space model (Rangapuram et al., 2018). However, these works usually study short-term forecasting and use RNNs that contain only the most recent state. Our method contrasts with this by explicitly modeling higher-order dynamics to capture long-term dependencies.

There are several classic work on higher-order RNNs. For example, (Giles et al., 1989) proposes a higher-order RNN to simulate a deterministic finite state machine and recognize regular grammars. The model considers a multiplicative structure of inputs and the most recent hidden state, but is limited to two-way interactions. (Sutskever et al., 2011) also studies tensor RNNs that allow a different hidden-to-hidden weight matrix for every input dimension. Soltani and Jiang (2016) proposes a higher-order RNN that concatenates a sequence of past hidden states, but the underlying state interactions are still linear. Moreover, hierarchical RNNs (Zheng et al., 2016) have been used to model sequential data at multiple temporal resolutions. Our method generalizes all these works to capture higher-order interactions using a hidden-to-hidden tensor.

Tensor methods Tensor methods have tight connections with neural networks. For example, (Novikov et al., 2015; Stoudenmire and Schwab, 2016) employ tensor-train to compress the weights in neural networks. (Yang et al., 2017) extends this idea to RNNs by reshaping the inputs into a tensor and factorizes the input-hidden weight tensor. However, the purpose of these works is model compression in the input space whereas our method learns the dynamics in the hidden state space. Theoretically, (Cohen et al., 2016) shows convolutional neural networks and hierarchical tensor factorizations are equivalent. (Khruikov et al., 2017) provides expressiveness analysis for shallow networks using tensor train.

Tensor methods have also been used for sequence modeling. For example, one can apply tensor decomposition as method of moments estimators for latent variable models such as Hidden Markov Models (HMMs) (Anandkumar et al., 2012). Tensor methods have also shown promises in reducing the model dimensionality of multivariate spatiotemporal learning problems (Yu and Liu, 2016), as well as nonlinear system identification (Decuyper et al., 2019). Most recently, Schlag and Schmidhuber (2018) combine tensor product of relational information and recurrent neural networks for natural language reasoning tasks. This work however, to the best of our knowledge, is the first to consider tensor networks within RNNs for sequence learning in environments with nonlinear dynamics.

3. Higher-Order Tensor RNNs

Forecasting Nonlinear Dynamics Our goal is to learn an efficient forecasting model for *continuous multivariate time series* in environments with nonlinear dynamics. The state $\mathbf{x}_t \in \mathbb{R}^d$ of such systems evolves over time using a set of *nonlinear* differential equations:

$$\left\{ \xi^i \left(\mathbf{x}_t, \frac{d\mathbf{x}}{dt}, \frac{d^2\mathbf{x}}{dt^2}, \dots; \phi \right) = 0 \right\}_i, \quad (1)$$

where ξ^i can be an arbitrary (smooth) function of the state \mathbf{x}_t and its derivatives. Continuous time dynamics are usually described by differential equations while difference equations

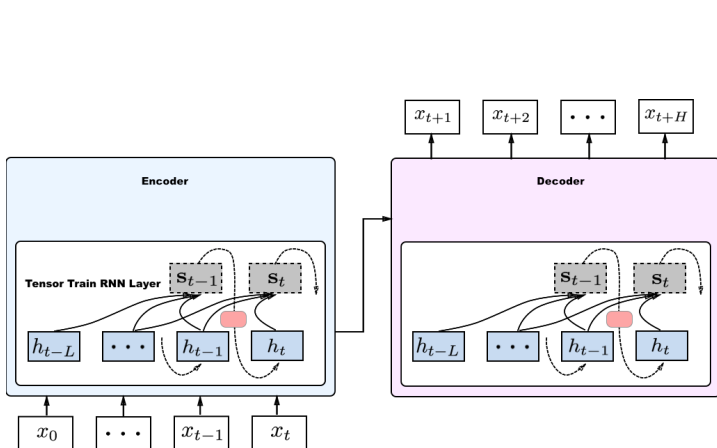


Figure 2: HOT-RNN within a seq2seq model. Both encoder and decoder contain higher-order recurrent cells. The augmented state \mathbf{s}_{t-1} (grey) takes in past L hidden states (blue) and forms a higher-order tensor. HOT-RNN (red) factorizes the tensor and outputs the next hidden state.

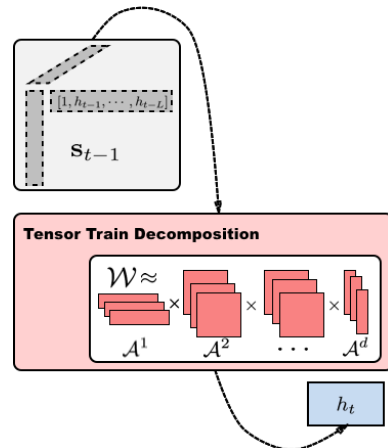


Figure 3: A HOT-RNN cell. The augmented state \mathbf{s}_{t-1} (grey) forms a higher-order tensor, which is then factorized to output the next hidden state.

are employed for discrete time. In continuous time, a classic example is the first-order Lorenz attractor, whose realizations showcase the “butterfly-effect”, a characteristic set of double-spiral orbits. In discrete-time, a non-trivial example is the 1-dimensional Genz dynamics, whose difference equation is:

$$x_{t+1} = (c^{-2} + (x_t + w)^2)^{-1}, \quad c, w \in [0, 1], \quad (2)$$

where x_t denotes the system state at time t and c, w are the parameters. Due to the nonlinear nature of the dynamics, such systems exhibit higher-order correlations, long-term dependencies and sensitivity to error propagation, and thus form a challenging setting for forecasting.

Given a sequence of initial states $\mathbf{x}_0 \dots \mathbf{x}_t$, the forecasting problem aims to learn a dynamics model F that outputs a sequence of future states $\mathbf{x}_{t+1} \dots \mathbf{x}_T$.

$$F : (\mathbf{x}_0 \dots \mathbf{x}_t) \mapsto (\mathbf{y}_t \dots \mathbf{y}_T), \quad \mathbf{y}_t = \mathbf{x}_{t+1}, \quad (3)$$

The system is governed by some unknown dynamics. Hence, accurately approximating the dynamics is critical to learning a good forecasting model and making predictions for long time horizons.

First-order Markovian Models In deep learning, popular approaches such as recurrent neural networks (RNNs) employ first-order hidden-state models to approximate the dynamics. An RNN with a single cell recursively computes a hidden state \mathbf{h}_t using the most recent hidden state \mathbf{h}_{t-1} , generating the output \mathbf{y}_t from the hidden state \mathbf{h}_t :

$$\mathbf{h}_t = f(\mathbf{x}_t, \mathbf{h}_{t-1}; \theta_f), \quad \mathbf{y}_t = g(\mathbf{h}_t; \theta_g), \quad (4)$$

where f is the state transition function, g is the output function and $\{\theta_f, \theta_g\}$ are the corresponding model parameters. A common parametrization scheme for (4) applies a nonlinear activation function such as sigmoid σ to a linear map of \mathbf{x}_t and \mathbf{h}_{t-1} as:

$$\mathbf{h}_t = \sigma(W^{hx}\mathbf{x}_t + W^{hh}\mathbf{h}_{t-1} + \mathbf{b}^h), \quad \mathbf{x}_{t+1} = W^{xh}\mathbf{h}_t + \mathbf{b}^x, \quad (5)$$

where W^{hx} , W^{xh} and W^{hh} are the transition weight matrices and \mathbf{b}^h , \mathbf{b}^x are the biases.

RNNs have many different variations, including LSTMs (Hochreiter and Schmidhuber, 1997) and GRUs (Chung et al., 2014). Although a RNN can approximate any function in theory, its hidden state \mathbf{h}_t only depends on the previous state \mathbf{h}_{t-1} and the input \mathbf{x}_t . Such models do not explicitly capture higher-order dynamics and only implicitly encode long-term dependencies between all historical states $\mathbf{h}_0 \dots \mathbf{h}_t$. This limits the representation power of RNNs, especially for forecasting in environments with nonlinear dynamics. Hence, instead of using a wide RNN with many hidden units, we exploit the recurrent cell to design higher-order tensor RNNs that can approximate complex non-linear governing equations.

3.1 Higher-Order Non-Markovian Models

To effectively learn nonlinear dynamics with higher-order temporal dependency, we propose a family of models that generalizes standard RNNs: higher-order recurrent neural networks, or HOT-RNN. We design HOT-RNNs with two goals in mind: explicitly modeling 1) L -order Markov processes with L steps of temporal memory and 2) polynomial interactions between the hidden states \mathbf{h} . and \mathbf{x}_t .

First, we consider longer ‘‘history’’: we keep length L historic states: $\mathbf{h}_t, \dots, \mathbf{h}_{t-L}$:

$$\mathbf{h}_t = f(\mathbf{x}_t, \mathbf{h}_{t-1}, \dots, \mathbf{h}_{t-L}; \theta_f) \quad (6)$$

where f represents the state transition function. In principle, early work (Giles et al., 1989) has shown that with a large enough hidden state size, such recurrent structures are capable of approximating any dynamical system.

Second, to learn the nonlinear dynamics ξ efficiently, we also use higher-order moments to approximate the state transition function. We use an augmented state \mathbf{s} , where we mute the subscript of \mathbf{s}_{t-1} for notation simplicity.:

$$\mathbf{s}^T = [1 \quad \mathbf{h}_{t-1}^T \quad \dots \quad \mathbf{h}_{t-L}^T] \quad (7)$$

which concatenates L previous hidden states. To compute \mathbf{h}_t , we construct a P -dimensional transition *weight tensor* to model degree- P polynomial interactions between hidden states:

$$[\mathbf{h}_t]_\alpha = \phi(W_\alpha^{hx}\mathbf{x}_t + \sum_{i_1, \dots, i_p} \mathcal{W}_{\alpha i_1 \dots i_p} \underbrace{\mathbf{s}_{i_1} \otimes \dots \otimes \mathbf{s}_{i_p}}_P)$$

where α indices the hidden dimension, i . indices the higher-order terms and P is the total polynomial order. We included the bias unit 1 in \mathbf{s} to account for the first order term, so that $\mathbf{s}_{i_1} \otimes \dots \otimes \mathbf{s}_{i_p} = [1, \mathbf{h}_t, \mathbf{h}_t \mathbf{h}_{t-1}, \dots]$ can include all polynomial expansions of hidden states up to order P .

The HOT-RNN with LSTM cell, or ‘‘HOT-LSTM’’, is defined analogously as:

$$[\mathbf{i}_t, \mathbf{g}_t, \mathbf{f}_t, \mathbf{o}_t]_\alpha = \sigma(W_\alpha^{hx} \mathbf{x}_t + \sum_{i_1, \dots, i_P} \mathcal{W}_{\alpha i_1 \dots i_P} \underbrace{\mathbf{s}_{i_1} \otimes \dots \otimes \mathbf{s}_{i_P}}_P), \quad (8)$$

$$\mathbf{c}_t = \mathbf{c}_{t-1} \circ \mathbf{f}_t + \mathbf{i}_t \circ \mathbf{g}_t, \quad \mathbf{h}_t = \mathbf{c}_t \circ \mathbf{o}_t$$

where \circ denotes the Hadamard product. Note that the bias units are again included.

HOT-RNN is a basic unit that can be incorporated in most of the existing recurrent neural architectures such as convolutional RNN (Xingjian et al., 2015) and hierarchical RNN (Chung et al., 2016). In this work, we use HOT-RNN as a module for sequence-to-sequence (seq2seq) framework (Sutskever et al., 2014) in order to perform long-term forecasting.

As shown in Figure 2, seq2seq models consist of an encoder-decoder pair. The encoder takes an input sequence and learns a hidden representation. The decoder initializes with this hidden representation and generates an output sequence. Both the encoder and the decoder contain multiple layers of higher-order tensor recurrent cells (red). The augmented state \mathbf{s}_{t-1} (grey) concatenates the past L hidden states; the HOT-RNN cell takes \mathbf{s}_{t-1} and outputs the next hidden state. The encoder encodes the initial states x_0, \dots, x_t and the decoder predicts x_{t+1}, \dots, x_T . For each time step t , the decoder uses its previous prediction \mathbf{y}_t as an input.

3.2 Dimension Reduction with Tensor-Train

Unfortunately, due to the ‘‘curse of dimensionality’’, the number of parameters in \mathcal{W}_α with hidden size H grows exponentially as $O(HL^P)$, which makes the higher-order model prohibitively large to train. To overcome this difficulty, we utilize *tensor networks* to approximate the weight tensor. Such networks encode a structural decomposition of tensors into low-dimensional components and have been shown to provide the most general approximation to smooth tensors (Orus, 2014). The most commonly used tensor networks are *linear tensor networks* (LTN), also known as *tensor-trains* in numerical analysis or *matrix-product states* in quantum physics (Oseledets, 2011).

A tensor train model decomposes a P -dimensional tensor \mathcal{W} into a network of sparsely connected low-dimensional tensors $\{\mathcal{A}^p \in \mathbb{R}^{r_{p-1} \times n_p \times r_p}\}$ as:

$$\mathcal{W}_{i_1 \dots i_P} = \sum_{\alpha_1 \dots \alpha_{P-1}} \mathcal{A}_{\alpha_0 i_1 \alpha_1}^1 \mathcal{A}_{\alpha_1 i_2 \alpha_2}^2 \dots \mathcal{A}_{\alpha_{P-1} i_P \alpha_P}^P$$

with $\alpha_0 = \alpha_P = 1$, as depicted in Figure (3). When $r_0 = r_P = 1$ the $\{r_p\}$ are called the tensor-train rank. With tensor-train decomposition, we can reduce the number of parameters of HOT-RNN from $(HL + 1)^P$ to $(HL + 1)R^2P$, with $R = \max_p r_p$ as the upper bound on the tensor-train rank. Thus, a major benefit of tensor-train is that they *do not* suffer from the curse of dimensionality, which is in sharp contrast to many classical tensor decomposition models, such as the Tucker decomposition.

4. Approximation Theorem for HOT-RNNs

A significant benefit of using HOT-RNN is that we can theoretically characterize its expressiveness for approximating the underlying dynamics. The main idea is to analyze a class

of functions that satisfies certain regularity conditions. For such functions, tensor-train representations preserve the weak differentiability and yield a compact representation.

The following theorem characterizes the representation power of HQT-RNN, viewed as a one-layer hidden neural network, in terms of 1) the regularity of the target function f , 2) the dimension of the input space, 3) the tensor train rank and 4) the order of the tensor:

Theorem 1 *Let the target function $f \in \mathcal{H}_\mu^k$ be a Hölder continuous function defined on a input domain $\mathcal{I} = I_1 \times \dots \times I_d$, with bounded derivatives up to order k and finite Fourier magnitude distribution C_f . A single layer HQT-RNN with h hidden units, \hat{f} can approximate f with approximation error ϵ at most:*

$$\epsilon \leq \frac{1}{h} \left(C_f^2 \frac{d-1}{(k-1)(r+1)^{k-1}} + C(k)p^{-k} \right) \quad (9)$$

where $C_f = \int |\omega|_1 |\hat{f}(\omega)| d\omega$, d is the dimension of the function, i.e., the size of the state space, r is the tensor-train rank, p is the degree of the higher-order polynomials i.e., the order of the tensor, and $C(k)$ is the coefficient of the spectral expansion of f .

Remarks: The result above shows that the number of weights required to approximate the target function f is dictated by its regularity (i.e., its Hölder-continuity order k). The expressiveness of HQT-RNN is driven by the selection of the rank r and the polynomial degree p ; moreover, it improves for functions with increasing regularity. Compared with “first-order” regular RNNs, HQT-RNNs are exponentially more powerful for large rank: if the order p increases, we require fewer hidden units h .

Proof sketch: For the full proof, see the Appendix. We design HQT-RNN to approximate the underlying system dynamics. The target function $f(\mathbf{x})$ represents the state transition function, as in (8). We first show that if f preserves weak derivatives, then it has a compact tensor-train representation. Formally, let us assume that f is a Sobolev function: $f \in \mathcal{H}_\mu^k$, defined on the input space $\mathcal{I} = I_1 \times I_2 \times \dots \times I_d$, where each I_i is a set of vectors. The space \mathcal{H}_μ^k is defined as the functions that have bounded derivatives up to some order k and are L_μ -integrable.

$$\mathcal{H}_\mu^k = \left\{ f \in L_\mu(\mathcal{I}) : \sum_{i \leq k} \|D^{(i)} f\|^2 < +\infty \right\}, \quad (10)$$

where $D^{(i)} f$ is the i -th weak derivative of f and $\mu \geq 0$.¹ It is known that any Sobolev function admits a Schmidt decomposition: $f(\cdot) = \sum_{i=0}^{\infty} \sqrt{\lambda_i} \gamma(\cdot)_i \otimes \phi(\cdot)_i$, where $\{\lambda\}$ are the eigenvalues and $\{\gamma\}, \{\phi\}$ are the associated eigenfunctions. Hence, for $\mathbf{x} \in \mathcal{I}$, we can represent the target function $f(\mathbf{x})$ as an infinite summation of products of a set of basis functions:

$$f(\mathbf{x}) = \sum_{\alpha_0, \dots, \alpha_d=1}^{\infty} \mathcal{A}^1(x_1)_{\alpha_0 \alpha_1} \cdots \mathcal{A}^d(x_d)_{\alpha_{d-1} \alpha_d}, \quad (11)$$

1. A weak derivative generalizes the derivative concept for (non)-differentiable functions and is implicitly defined as: e.g. $v \in L^1([a, b])$ is a weak derivative of $u \in L^1([a, b])$ if for all smooth φ with $\varphi(a) = \varphi(b) = 0$: $\int_a^b u(t) \varphi'(t) dt = - \int_a^b v(t) \varphi(t) dt$.

where $\{\mathcal{A}^j(x_j)_{\alpha_{j-1}\alpha_j}\}$ are basis functions over each input dimension. These basis functions satisfy $\langle \mathcal{A}^j(\cdot)_{im}, \mathcal{A}^j(\cdot)_{in} \rangle = \delta_{mn}$ for all j . If we truncate (11) to a low dimensional subspace ($\mathbf{r} < \infty$), we obtain a functional approximation of the state transition function $f(\mathbf{x})$. This approximation is also known as the *functional tensor-train* (FTT):

$$f_{FTT}(\mathbf{x}) = \sum_{\alpha_0, \dots, \alpha_d}^{\mathbf{r}} \mathcal{A}^1(x_1)_{\alpha_0\alpha_1} \cdots \mathcal{A}^d(x_d)_{\alpha_{d-1}\alpha_d}, \quad (12)$$

In practice, HOT-RNN implements a polynomial expansion of the states using $[\mathbf{s}, \mathbf{s}^{\otimes 2}, \dots, \mathbf{s}^{\otimes P}]$, where P is the degree of the polynomial. The final function represented by HOT-RNN is a polynomial approximation of the functional tensor-train function f_{FTT} .

Given a target function $f(\mathbf{x}) = f(\mathbf{s} \otimes \cdots \otimes \mathbf{s})$, we can express it using FTT and the polynomial expansion of the states \mathbf{s} . This allows us to characterize HOT-RNN using a family of functions that it can represent. Combined with the classic neural network approximation theory Barron (1993), we can bound the approximation error for HOT-RNN with one hidden layer. The above results applies to the full family of HOT-RNNs, including those using vanilla RNN or LSTM as the recurrent cell.

One can think of the universal approximation result in Theorem 1 bounds the estimation bias of the model: $f - \mathbb{E}[\hat{f}]$, where the expectation is taken over training sets. While a large neural network can approximate any function, training as a large neural network will be hard given a finite data set, demonstrating bias-variance trade-off. In the next section, we provide bounds for the estimation variance.

5. Variance Bound for HOT-RNN

Given a time series from a P -th order dynamics (X_1, \dots, X_P) , denote the variance over the joint hidden states as $\hat{C} := \sum_{i=1}^m \otimes [\mathcal{A}(X_1^{(i)}), \dots, \mathcal{A}(X_P^{(i)})]$, where $\mathcal{A}(\cdot)$ are the basis functions. Define the variance of the estimated dynamics as $C := \mathbb{E}_{X_1 X_2 \dots, X_P} [\phi(X_1) \otimes \phi(X_2), \dots, \otimes \phi(X_P)]$, with $\phi(\cdot)$ being the feature mapping. The following theorem bounds the estimation variance of the HOT-RNN.

Theorem 2 (Estimation Variance Bound) *Assuming the time series is governed by a system whose order of dynamics is at most P , represented as a joint probabilistic distribution $P(X_1, \dots, X_P)$. The variance for the HOT-RNN estimator \hat{C} and the true variance C of the population statistics is upper bounded by:*

$$\|\hat{C} - C\| = \mathcal{O}_p\left(\frac{2\sqrt{2}\rho^{P/2}\sqrt{\log \frac{2}{\delta}}}{\sqrt{m}}\right)$$

where $C := \mathbb{E}_{X_1 X_2 \dots, X_P} [\phi(X_1) \otimes \phi(X_2), \dots, \otimes \phi(X_P)]$ and m is number of samples, $\rho := \sup_{x \in \mathcal{X}} k(x, x)$.

Proof : The tensor-train distribution forms a Gibbs field, thus based on Hammersley-Clifford Theorem, a Gibbs field satisfies global Markov property, therefore, it must be a Conditional Random Field (CRF) as the conditional probability distribution factorizes. According to the duality between tensor network and graphical model Robeva and Seigal

(2017), tensor train is the dual graph of CRF. Figure 4 visualizes such dual relationship in the graphical model template. After establishing the relationship between conditional random field and functional tensor-train, we can bound the variance of the HOT-RNN estimator.

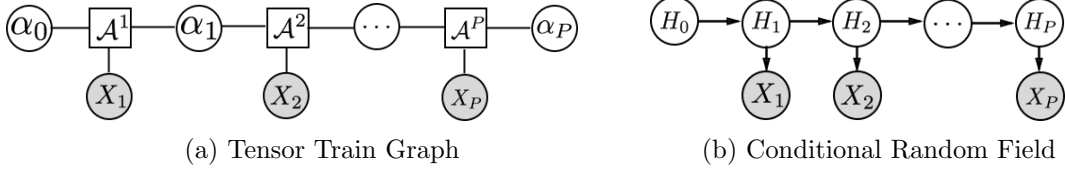


Figure 4: The graphical representation of tensor train model and conditional random field. The circles denote hidden variables and the shaded circles represent observed variables.

We first state the well-celebrated Hammersley-Clifford theorem that gives the sufficient and necessary conditions of which a probability distribution is a Markov Random field.

Theorem 3 (Hammersley-Clifford) *A graphical model G is a Markov Random Field if and only if the probability distribution $P(X)$ on G is a Gibbs distribution:*

$$P(X) = \frac{1}{Z} \prod_{c \in C_G} \psi(X_c)$$

where $Z = \sum_x \prod_{c \in C_G} \psi(X_c)$ is the normalization constant, ψ are functions defined on maximal cliques, and C_G is a set of all maximal cliques in the graph.

When the underlying distribution is a Markov random field and belongs to the exponential family, we can generalize Theorem 3 to kernel functions and obtain the following results.

Lemma 4 (Kernelized Hammersley-Clifford) *Altun et al. (2012) Given a Markov random field X with respect to a graphical model G , if the sufficient statistics $\Phi(X) = (\Phi(X_{c_1}), \dots, \Phi(X_{c_i}))$, then the kernels $k(X, X') = \langle \Phi(X), \Phi(X') \rangle$ satisfy*

$$k(X, X') = \sum_{c \in C_G} k_c(X_c, X'_c)$$

where $\Phi(X_c)$ are the sufficient statistics defined on maximal cliques, $k_c(X, X') = \langle \Phi(X_c), \Phi(X'_c) \rangle$

Our tensor train model factorizes the state transition function $\mathbf{h}_t = \mathbf{x}_t + f(\mathbf{s}_1 \otimes \dots \otimes \mathbf{s}_p)$, where each augmented hidden states $\mathbf{s} = [1, \mathbf{h}_{t-1}, \dots, \mathbf{h}_{t-L}]$. For a joint distribution of d variables X_1, \dots, X_P , taking values from 1 to n from a conditional random field. Their joint probability density table is a d -dimensional tensor $P(X_1, \dots, X_P) \in \mathbb{R}^{n^P}$, with the values of the variable act as indices. Following the result of Lemma 4, the feature functions $\mathcal{A}(X_p)$ factorize over maximum cliques:

$$\begin{aligned} P(X_1, \dots, X_P) &= \sum_{\alpha_0, \dots, \alpha_P} P(X_1, \dots, X_d, \alpha_0, \dots, \alpha_P) \\ &= \sum_{\alpha_0, \dots, \alpha_P=1}^{\infty} \mathcal{A}^1(X_1)_{\alpha_0 \alpha_1} \dots \mathcal{A}^d(X_d)_{\alpha_{P-1} \alpha_P}, \end{aligned}$$

which is the functional tensor-train model.

Consider a time series of dynamics up to P -th order, we can view the time series as a joint distribution over P variables $P(X_1, X_2, \dots, X_P)$. The covariance of such joint distribution is defined as $C := \mathbb{E}_{X_1 X_2 \dots, X_P}[\phi(X_1) \otimes \phi(X_2), \dots, \otimes \phi(X_P)]$. HOT-RNN estimates the joint distribution by factorizing the tensor product of the feature mapping functions: $\hat{C} := \sum_{i=1}^m \otimes [\mathcal{A}(X_1^{(i)}), \dots, \mathcal{A}(X_P^{(i)})]$. Given m i.i.d. samples of times series, $\mathcal{D} = \{X_1^{(i)}, X_2^{(i)}, \dots, X_P^{(i)}\}_{i=1}^m$, we can then generalize the results from Song et al. (2013) for multi-view latent variable models to HOT-RNN.

6. Experiments

We conducted exhaustive experiments to examine the behavior of the proposed HOT-RNN model on both synthetic and real-world time series data. The source code is available at https://github.com/yuqirose/tensor_train_RNN.

6.1 Datasets

We validated the accuracy and efficiency of HOT-RNN on the following three datasets.

Genz Genz functions are often used as basis for evaluating high-dimensional function approximation. In particular, they have been used to analyze tensor-train decompositions (Bigoni et al., 2016). There are in total 7 different Genz functions. (1) $g_1(x) = \cos(2\pi w + cx)$, (2) $g_2(x) = (c^{-2} + (x + w)^{-2})^{-1}$, (3) $g_3(x) = (1 + cx)^{-2}$, (4) $e^{-c^2\pi(x-w)^2}$ (5) $e^{-c^2\pi|x-w|}$ (6) $g_6(x) = \begin{cases} 0 & x > w \\ e^{cx} & else \end{cases}$. For each function, we generated a dataset with 10,000 samples using (2) with $w = 0.5$ and $c = 1.0$ and random initial points draw from a range of $[-0.1, 0.1]$.

Traffic We use the traffic data of Los Angeles County highway network collected from California department of transportation ². The dataset consists of 4 month speed readings aggregated every 5 minutes. Due to large number of missing values ($\sim 30\%$) in the raw data, we impute the missing values using the average values of non-missing entries from other sensors at the same time. In total, after processing, the dataset covers 35 136, time-series. We treat each sequence as daily traffic of 288 time stamps. We up-sample the dataset every 20 minutes, which results in a dataset of 8 784 sequences of daily measurements. We select 15 sensors as a joint forecasting tasks.

Climate We use the daily maximum temperature data from the U.S. Historical Climatology Network (USHCN) daily ³. The dataset contains daily measurements for 5 climate variables for approximately 124 years. The records were collected across more than 1 200 locations and span over 45 384 days. We analyze the area in California which contains 54 stations. We removed the first 10 years of day, most of which has no observations. We treat the temperature reading per year as one sequence and impute the missing observations using other non-missing entries from other stations across years. We augment the datasets by rotating the sequence every 7 days, which results in a data set of 5 928 sequences.

2. <http://pems.dot.ca.gov/>

3. http://cdiac.ornl.gov/ftp/ushcn_daily/

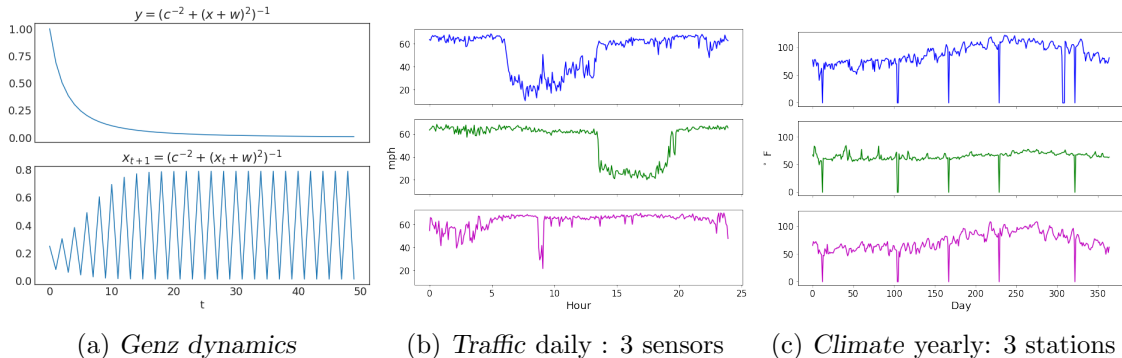


Figure 5: Data visualizations: (13) Genz dynamics, (5b) traffic data, (5c) climate data.

Figure 5 visualizes the time series from Genz dynamics, traffic and climate systems, respectively. To test the stationarity of the time series, we also perform a DickeyFuller test on the real-world traffic and climate data. DickeyFuller test is a commonly used statistical test procedure to determine whether a time series is stationary. Its null hypothesis is that a unit root is present in an autoregressive model, hence the time series is not stationary. The test statistics of the traffic and climate data is shown in Table 1, which demonstrate the non-stationarity of the time series.

	Traffic		Climate	
Test Statistic	0.00003	0	3e-7	0
p-value	0.96	0.96	1.12 e-13	2.52 e-7
Number Lags Used	2	7	0	1
Critical Value (1%)	-3.49	-3.51	-3.63	2.7
Critical Value (5%)	-2.89	-2.90	-2.91	-3.70
Critical Value (10%)	-2.58	-2.59	-2.60	-2.63

Table 1: Dickey-Fuller test statistics for traffic and climate data used in the experiments.

6.2 Training Details

Setup We use a seq2seq architecture with HOT-RNN using LSTM as recurrent cells (HOT-LSTM). For all experiments, we use the length- T sequence regression loss $L(y, \hat{y}) = \sum_{t=1}^T \|\hat{y}_t - y_t\|_2^2$, where $y_t = x_{t+1}$, \hat{y}_t are the ground truth and model prediction respectively. For all datasets, we used a 80% – 10% – 10% train-validation-test split and train for a maximum of $1e^4$ steps. We compute the moving average of the validation loss as an early stopping criteria. We also did not include scheduled sampling Bengio et al. (2015), as we found training with scheduled sampling became highly unstable under a range of annealing schedules.

Hyperparameter Search All models are trained using RMS-prop with a learning rate decay of 0.8. We performed an exhaustive search over the hyper-parameters for validation. Table 2 reports the search range of different hyper-parameters used in this work.

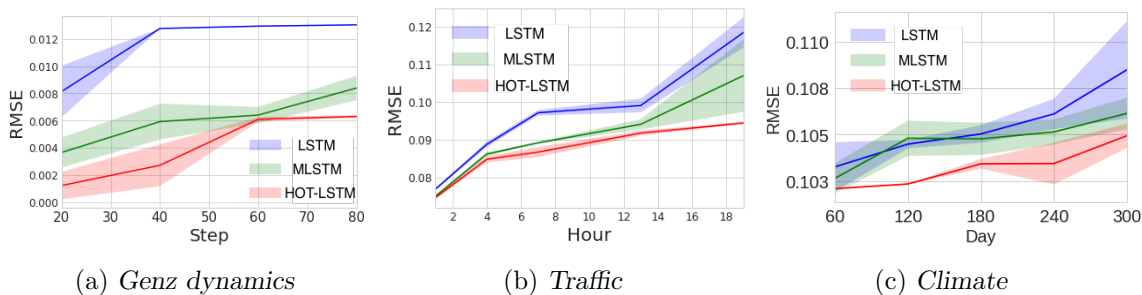


Figure 6: Long-term forecasting RMSE for *Genz dynamics* and real world *traffic*, *climate* time series (best viewed in color). Comparison of LSTM, MLSTM, and HOT-LSTM for varying forecasting horizons given same initial inputs. Results are averaged over 3 runs.

Hyper-parameter search range			
learning rate	$10^{-1} \dots 10^{-5}$	hidden state size	8, 16, 32, 64, 128
tensor-train rank	1 ... 16	number of lags	1 ... 6
number of orders	1 ... 3	number of layers	1 ... 3

Table 2: Hyper-parameter search range statistics for HOT-RNN experiments.

Baselines We compared HOT-RNN against 2 sets of natural baselines: 1st-order RNN (vanilla RNN, LSTM), and matrix RNNs (vanilla MRNN, MLSTM), which use matrix products of multiple hidden states without factorization (Soltani and Jiang, 2016). We observed that HOT-RNN with RNN cells outperforms vanilla RNN and MRNN, but using LSTM cells performs best in all experiments. We also evaluated the classic ARIMA time series model with AR lags of 1 ~ 5, and MA lags of 1 ~ 3. We observed that it consistently performs ~ 5% worse than LSTM.

6.3 Long-term Forecasting Accuracy

We evaluate the long-term forecasting accuracy of the proposed method and the baselines. For *traffic*, we forecast up to 18 hours ahead with 5 hours as inputs. For *climate*, we forecast up to 300 days ahead given 60 days of observations. For *Genz dynamics*, we forecast for 80 steps given 5 initial steps. We report the forecasting results averaged over 3 runs.

Figure 6 shows the test prediction error (in RMSE) for varying forecasting horizons for different datasets. We can see that HOT-LSTM notably outperforms all baselines on all datasets in this setting. In particular, HOT-LSTM is more robust to long-term error propagation. We observe two salient benefits of using HOT-RNNs over the unfactorized models.

First, MRNN and MLSTM can suffer from overfitting as the number of weights increases. Second, on *traffic*, unfactorized models also show considerable instability in their long-term predictions. These results suggest that HOT-RNNs learn more stable repre-

	Moving-MNIST (RMSE $\times 10^{-2}$)		
	LSTM	MLSTM	HOT-LSTM
$T = 20$	9.45	9.92	8.94
$T = 40$	10.04	9.94	9.92

Table 3: Sequence-averaged per-pixel RMSE on Moving MNIST.

sentations that generalize better for long-term horizons. To compare the performance on high-dimensional time series, we also evaluated on the unsupervised video prediction task for *Moving MNIST*. We forecast 20 and 40 frames ahead given 10 initial frames. The per-pixel forecasting RMSE results are shown in Table 3. We observe a small gain ($\sim 2 - 5\%$) of HOT-LSTM over the baselines. This is likely due to the fact that the underlying circular dynamics are still pretty simple. Moreover, the high-dimensional inputs have spatial structure that are hard to learn by RNNs alone (note we do not use convolutional features). We expect HOT-LSTM to improve over baselines even more with more complicated dynamics and using convolutional features.

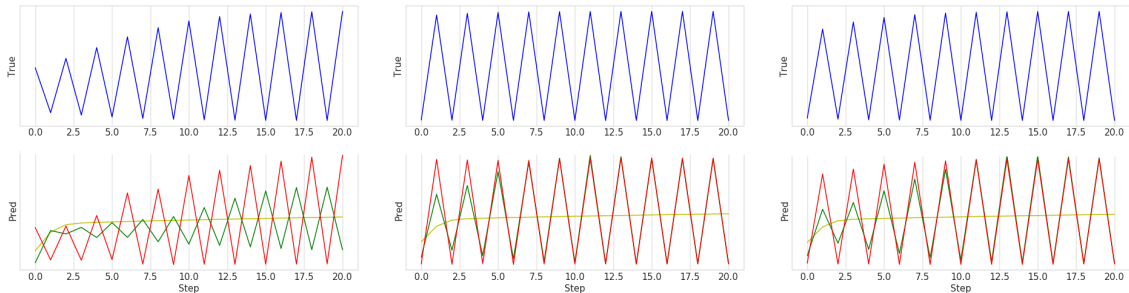


Figure 7: Model prediction for three Genz dynamics “product peak” with different initial conditions. Top (blue): ground truth. Bottom: model predictions for LSTM (green) and HOT-LSTM (red). HOT-LSTM perfectly captures the Genz oscillations, whereas the LSTM fails to do so (left) or only approaches the ground truth towards the end (middle and right).

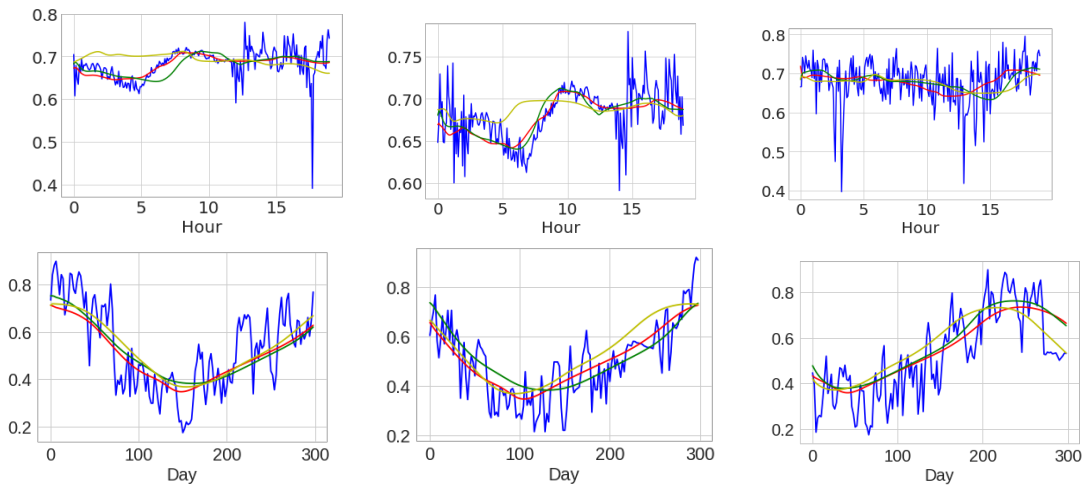


Figure 8: Top: 18 hour ahead predictions for hourly *traffic* time series given 5 hour as input for LSTM, MLSTM and HOT-LSTM. Bottom: 300 days ahead predictions for daily *climate* time series given 2 month observations as input for LSTM, MLSTM and HOT-LSTM.

6.4 Visualization of Predictions

To get intuition for the learned models, we visualize predictions from the best performing HOT-LSTM and baselines. Figure 7 shows the predictions for the Genz function “corner-peak” as the state-transition function from three realizations of Genz dynamics. We can see that HOT-LSTM can almost perfectly recover the original function, while LSTM and MLSTM only correctly predict the mean. These baselines cannot capture the dynamics fully, often predicting an incorrect range and phase for the dynamics.

Figure 8 shows predictions for the traffic and climate datasets. This work uses deterministic models, hence the predictions correspond to the trend. We can see that the HOT-LSTM aligns significantly better with ground truth in long-term forecasting. As the ground truth time series is highly nonlinear and noisy, LSTM often deviates from the general trend. While both MLSTM and HOT-LSTM can correctly learn the trend, HOT-LSTM captures more detailed curvatures due to higher-order structure.

6.5 Model Capacity

The number of parameters for HOT-RNN is $\mathcal{O}(HL + 1)R^2P$ with hidden size H , lag L , rank R and order P . This gives us more flexibility to decide the model capacity. Fewer parameters may have limited representation power, while more parameters would cause overfitting. Note that the memory complexity only grows quadratically with the rank R while Theorem 1 shows the expressiveness of HOT-RNN improves exponentially. In practice, we used cross-validation to select the values for these hyperparameters. The best models on real-world climate and traffic data are listed in Table 4. We can see that the number of parameters of HOT-LSTM model is comparable with that of MLSTM and LSTM.

Table 4: Best performing model size on traffic and climate data.

Number of Parameters			
TLSTM	MLSTM	LSTM	
7,200	9,700	8,700	

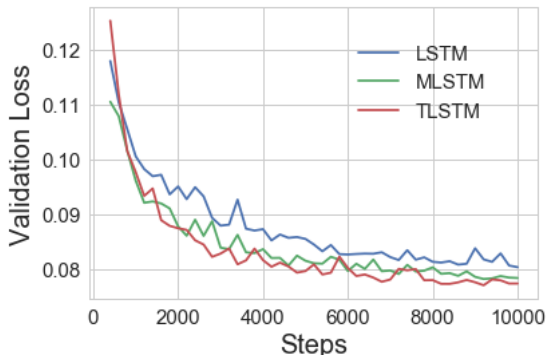


Figure 9: Training speed evaluation of different models: validation loss versus number of steps. Results are reported using the models with the best long-term forecasting accuracy.

HOT-LSTM Prediction Error (RMSE $\times 10^{-2}$)				
RANK r	2	4	8	16
GENZ ($T = 95$)	0.82	0.93	1.01	1.01
TRAFFIC ($T = 67$)	9.17	9.11	9.32	9.31
CLIMATE ($T = 360$)	10.55	10.25	10.51	10.63

Table 5: HOT-LSTM performance for varying tensor rank r with $L = 3$.

HOT-LSTM Traffic Prediction Error (RMSE $\times 10^{-2}$)				
LAGS L	2	4	5	6
$T = 12$	7.38	7.41	7.43	7.41
$T = 84$	8.97	9.31	9.38	9.01
$T = 156$	9.49	9.32	9.48	9.31
$T = 228$	10.19	9.63	9.58	9.94

Table 6: HOT-LSTM performance for various lags L and prediction horizons T .

6.6 Speed Performance Trade-off

We now investigate potential trade-offs between accuracy and computation. Figure 9 displays the validation loss with respect to the number of steps, for the best performing models on long-term forecasting. We see that H_OT-RNNs converge faster than other models, and achieve lower validation-loss. This suggests that H_OT-RNN has a more efficient representation of the nonlinear dynamics, and can learn much faster as a result.

6.7 Sensitivity Analysis

The H_OT-LSTM model has several hyperparameters, such as tensor-train rank and lag L . We study the sensitivity of H_OT-LSTM to these hyperparameters; Table 5 shows the results. In the top row, we report the prediction RMSE for the largest forecasting horizon w.r.t tensor ranks for all the datasets with lag 3. When the rank is too low, the model does not have enough capacity to capture non-linear dynamics. When the rank is too high, the model starts to overfit. In the bottom row, we report the effect of changing lag L . For each setting, the best r is determined by cross-validation. Note that the best lag L also varies for different forecasting horizons.

6.8 Chaotic Nonlinear Dynamics

Chaotic dynamics such as Lorenz attractor is notoriously difficult to learn in non-linear dynamics. In such systems, the dynamics are highly sensitive to perturbations in the input state: two close points can move exponentially far apart under the dynamics. We also evaluated tensor-train neural networks on long-term forecasting for Lorenz attractor and report the results.

Lorenz The Lorenz attractor system describes a two-dimensional flow of fluids:

$$\frac{dx}{dt} = \sigma(y - x), \quad \frac{dy}{dt} = x(\rho - z) - y, \quad \frac{dz}{dt} = xy - \beta z, \quad \sigma = 10, \rho = 28, \beta = 2.667.$$

This system has chaotic solutions (for certain parameter values) that revolve around the so-called Lorenz attractor. We simulated 10 000 trajectories with the discretized time interval length 0.01. We sample from each trajectory every 10 units in Euclidean distance. As shown in Figure 10, the blue trajectory represents the discretized dynamics and red circles are sampled observations. The dynamics is generated using $\sigma = 10$, $\rho = 28$, $\beta = 2.667$. The initial condition of each trajectory is sampled uniformly random from the interval of $[-0.1, 0.1]$.

Figure 11 shows 45 steps ahead predictions for all models. HORNN is the full tensor H_OT-RNN using vanilla RNN unit without the tensor-train decomposition. We can see all the tensor models perform better than vanilla RNN or MRNN. H_OT-RNN shows slight improvement at the beginning state.

We have also evaluated H_OT-RNN on long-term forecasting for *chaotic* dynamics, such as the Lorenz dynamics. Such dynamics are highly sensitive to input perturbations: two

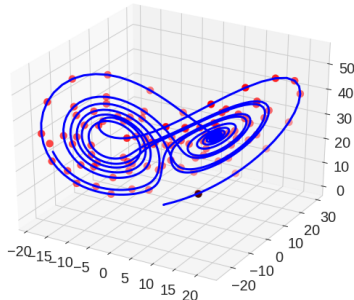


Figure 10: Lorenz Attractor

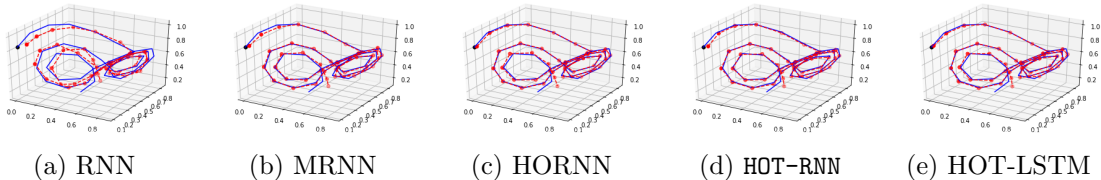


Figure 11: Long-term (right 2) predictions for different models (red) versus the ground truth (blue). **HOT-RNN** shows more consistent, but imperfect, predictions, whereas the baselines are highly unstable and gives noisy predictions.

close points can move exponentially far apart under the dynamics. This makes long-term forecasting highly challenging, as small errors can lead to catastrophic long-term errors. Figure 12 shows that **HOT-RNN** can predict up to $T = 40$ steps into the future, but diverges quickly beyond that. We have found no state-of-the-art prediction model is stable beyond 40 time step in this setting.

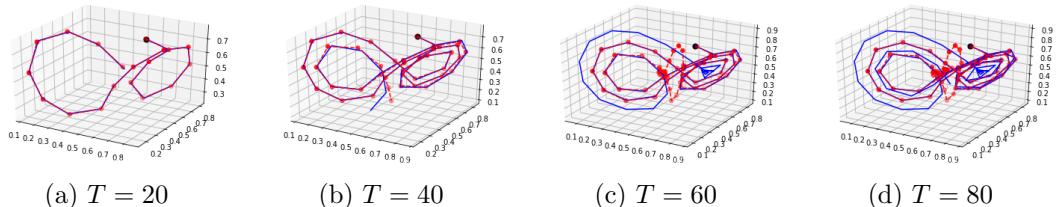


Figure 12: 10 Lorenz attraction with dynamics (blue) and sampled data (red). 12a, 12b, 12c, 12d **HOT-LSTM** long-term predictions for different forecasting horizons T versus the ground truth (blue). **HOT-LSTM** shows consistent predictions over increasing horizons T .

7. Discussion

In this paper, We studied long-term forecasting under nonlinear dynamics. We proposed a novel class of RNNs – **HOT-RNN** that directly learns the nonlinear dynamics using higher-order structures. We provided the first approximation guarantees for its representation power. We demonstrated the benefits of **HOT-RNN** to forecast accurately for significantly longer time horizon in both synthetic and real-world multivariate time series data.

In terms of future work, forecasting *chaotic dynamics*, still presents a significant challenge to any sequential prediction model. Hence, it would be worthwhile to study how to learn robust models for chaotic dynamics. For other sequence modeling tasks, such as language, there does not (or is not known to) exist a succinct analytical description of the data-generating process. It would also be interesting to go beyond forecasting and further investigate the effectiveness of **HOT-RNNs** in such domains as well.

Acknowledgments

We would like to acknowledge support for this project from the National Science Foundation (NSF grant IIS-9988642) and the Multidisciplinary Research Program of the Department of Defense (MURI N00014-00-1-0637).

References

- Yasemin Altun, Alex Smola, and Thomas Hofmann. Exponential families for conditional random fields. *arXiv preprint arXiv:1207.4131*, 2012.
- Animashree Anandkumar, Daniel Hsu, and Sham M Kakade. A method of moments for mixture models and hidden markov models. In *Conference on Learning Theory*, pages 33–1, 2012.
- Andrew R Barron. Universal approximation bounds for superpositions of a sigmoidal function. *IEEE Transactions on Information theory*, 39(3):930–945, 1993.
- Samy Bengio, Oriol Vinyals, Navdeep Jaitly, and Noam Shazeer. Scheduled sampling for sequence prediction with recurrent neural networks. In *Advances in Neural Information Processing Systems*, pages 1171–1179, 2015.
- Daniele Bigoni, Allan P Engsig-Karup, and Youssef M Marzouk. Spectral tensor-train decomposition. *SIAM Journal on Scientific Computing*, 38(4):A2405–A2439, 2016.
- George EP Box, Gwilym M Jenkins, Gregory C Reinsel, and Greta M Ljung. *Time series analysis: forecasting and control*. John Wiley & Sons, 2015.
- Junyoung Chung, Caglar Gulcehre, KyungHyun Cho, and Yoshua Bengio. Empirical evaluation of gated recurrent neural networks on sequence modeling. *arXiv preprint arXiv:1412.3555*, 2014.
- Junyoung Chung, Sungjin Ahn, and Yoshua Bengio. Hierarchical multiscale recurrent neural networks. *arXiv preprint arXiv:1609.01704*, 2016.
- Nadav Cohen, Or Sharir, and Amnon Shashua. On the expressive power of deep learning: a tensor analysis. In *29th Annual Conference on Learning Theory*, pages 698–728, 2016.
- Jan Decuyper, Philippe Dreesen, Johan Schoukens, Mark C Runacres, and Koen Tiels. Decoupling multivariate polynomials for nonlinear state-space models. *IEEE Control Systems Letters*, 2019.
- Carlton Downey, Ahmed Hefny, and Geoffrey Gordon. Practical learning of predictive state representations. *arXiv preprint arXiv:1702.04121*, 2017.
- Valentin Flunkert, David Salinas, and Jan Gasthaus. Deepar: Probabilistic forecasting with autoregressive recurrent networks. *arXiv preprint arXiv:1704.04110*, 2017.
- C Lee Giles, Guo-Zheng Sun, Hsing-Hen Chen, Yee-Chun Lee, and Dong Chen. Higher order recurrent networks and grammatical inference. In *NIPS*, pages 380–387, 1989.
- Sepp Hochreiter and Jürgen Schmidhuber. Long short-term memory. *Neural computation*, 9(8):1735–1780, 1997.
- Valentin Khrulkov, Alexander Novikov, and Ivan Oseledets. Expressive power of recurrent neural networks. *arXiv preprint arXiv:1711.00811*, 2017.

- Yann LeCun, Yoshua Bengio, and Geoffrey Hinton. Deep learning. *Nature*, 521(7553): 436–444, 2015.
- Lennart Ljung. System identification. *Wiley Encyclopedia of Electrical and Electronics Engineering*, 2001.
- Alexander Novikov, Dmitrii Podoprikin, Anton Osokin, and Dmitry P Vetrov. Tensorizing neural networks. In *Advances in Neural Information Processing Systems*, pages 442–450, 2015.
- Román Orús. A practical introduction to tensor networks: Matrix product states and projected entangled pair states. *Annals of Physics*, 349:117–158, 2014.
- Ivan V Oseledets. Tensor-train decomposition. *SIAM Journal on Scientific Computing*, 33(5):2295–2317, 2011.
- Syama Sundar Rangapuram, Matthias W Seeger, Jan Gasthaus, Lorenzo Stella, Yuyang Wang, and Tim Januschowski. Deep state space models for time series forecasting. In *Advances in Neural Information Processing Systems*, pages 7785–7794, 2018.
- Elina Robeva and Anna Seigal. Duality of graphical models and tensor networks. *arXiv preprint arXiv:1710.01437*, 2017.
- Imanol Schlag and Jürgen Schmidhuber. Learning to reason with third order tensor products. In *Advances in Neural Information Processing Systems*, pages 9981–9993, 2018.
- Jürgen Schmidhuber. Deep learning in neural networks: An overview. *Neural networks*, 61: 85–117, 2015.
- Rohollah Soltani and Hui Jiang. Higher order recurrent neural networks. *arXiv preprint arXiv:1605.00064*, 2016.
- Hagen Soltau, Hank Liao, and Hasim Sak. Neural speech recognizer: Acoustic-to-word lstm model for large vocabulary speech recognition. *arXiv preprint arXiv:1610.09975*, 2016.
- Le Song, Animashree Anandkumar, Bo Dai, and Bo Xie. Nonparametric estimation of multi-view latent variable models. *arXiv preprint arXiv:1311.3287*, 2013.
- Nitish Srivastava, Elman Mansimov, and Ruslan Salakhudinov. Unsupervised learning of video representations using lstms. In *International conference on machine learning*, pages 843–852, 2015.
- Edwin Stoudenmire and David J Schwab. Supervised learning with tensor networks. In *Advances in Neural Information Processing Systems*, pages 4799–4807, 2016.
- Ilya Sutskever, James Martens, and Geoffrey E Hinton. Generating text with recurrent neural networks. In *Proceedings of the 28th International Conference on Machine Learning (ICML-11)*, pages 1017–1024, 2011.
- Ilya Sutskever, Oriol Vinyals, and Quoc V Le. Sequence to sequence learning with neural networks. In *Advances in neural information processing systems*, pages 3104–3112, 2014.

- SHI Xingjian, Zhouong Chen, Hao Wang, Dit-Yan Yeung, Wai-Kin Wong, and Wang-chun Woo. Convolutional lstm network: A machine learning approach for precipitation nowcasting. In *Advances in neural information processing systems*, pages 802–810, 2015.
- Yinchong Yang, Denis Krompass, and Volker Tresp. Tensor-train recurrent neural networks for video classification. In *International Conference on Machine Learning*, pages 3891–3900, 2017.
- Rose Yu and Yan Liu. Learning from multiway data: Simple and efficient tensor regression. In *International Conference on Machine Learning*, 2016.
- Stephan Zheng, Yisong Yue, and Patrick Lucey. Generating long-term trajectories using deep hierarchical networks. In *Advances in Neural Information Processing Systems*, pages 1543–1551, 2016.

Appendix A.

.1 Theoretical Analysis

We provide theoretical guarantees for the proposed HQT-RNN model by analyzing a class of functions that satisfy some regularity condition. For such functions, tensor-train decomposition preserve weak differentiability and yield a compact representation. We combine this property with neural network theory to bound the approximation error for HQT-RNN with one hidden layer, in terms of: 1) the regularity of the target function f , 2) the dimension of the input, and 3) the tensor train rank.

In the context of HQT-RNN, the target function $f(\mathbf{x})$ with $\mathbf{x} = \mathbf{s} \otimes \dots \otimes \mathbf{s}$, is the system dynamics that describes state transitions. Let us assume that $f(\mathbf{x})$ is a Sobolev function: $f \in \mathcal{H}_\mu^k$, defined on the input space $\mathcal{I} = I_1 \times I_2 \times \dots \times I_d$, where each I_i is a set of vectors. The space \mathcal{H}_μ^k is defined as the set of functions that have bounded derivatives up to some order k and are L_μ -integrable:

$$\mathcal{H}_\mu^k = \left\{ f \in L_\mu^2(I) : \sum_{i \leq k} \|D^{(i)} f\|^2 < +\infty \right\}, \quad (13)$$

where $D^{(i)} f$ is the i -th weak derivative of f and $\mu \geq 0$.⁴

Any Sobolev function admits a Schmidt decomposition: $f(\cdot) = \sum_{i=0}^{\infty} \sqrt{\lambda_i} \gamma(\cdot)_i \otimes \phi(\cdot)_i$, where $\{\lambda\}$ are the eigenvalues and $\{\gamma\}, \{\phi\}$ are the associated eigenfunctions. Applying the Schmidt decomposition along x_1 , we have

$$f(\mathbf{x}) = \sum_{\alpha_1} \sqrt{\lambda_{\alpha_1}} \gamma(x_1)_{\alpha_1} \phi(x_2, \dots, x_d)_{\alpha_1} \quad (14)$$

We can apply similar Schmidt decomposition along x_2

$$\sqrt{\lambda_{\alpha_1}} \phi(x_2, \dots, x_d)_{\alpha_1} = \sum_{\alpha_2} \sqrt{\lambda_{\alpha_2}} \gamma(x_2)_{\alpha_1, \alpha_2} \phi(x_3, \dots, x_d)_{\alpha_2} \quad (15)$$

Recursively performing such operation, and let $\gamma(x_d)_{\alpha_{d-1}, \alpha_d} = \sqrt{\lambda_{\alpha_{d-1}}} \phi(x_d)_{\alpha_{d-1}}$ and $\mathcal{A}^j(x_j)_{\alpha_{j-1}, \alpha_j} = \gamma(x_j)_{\alpha_{j-1}, \alpha_j}$, the target function $f \in \mathcal{H}_\mu^k$ can be decomposed as:

$$f(\mathbf{x}) = \sum_{\alpha_0, \dots, \alpha_d=1}^{\infty} \mathcal{A}^1(x_1)_{\alpha_0 \alpha_1} \dots \mathcal{A}^d(x_d)_{\alpha_{d-1} \alpha_d}, \quad (16)$$

where $\{\mathcal{A}^j(\cdot)_{\alpha_{j-1}, \alpha_j}\}$ are basis functions, satisfying $\langle \mathcal{A}^j(\cdot)_{im}, \mathcal{A}^j(\cdot)_{in} \rangle = \delta_{mn}$. We can truncate Eqn 17 to a low dimensional subspace ($\mathbf{r} < \infty$), and obtain the *functional tensor-train (FTT)* approximation of the target function f :

$$f_{TT}(\mathbf{x}) = \sum_{\alpha_0, \dots, \alpha_d=1}^{\mathbf{r}} \mathcal{A}^1(x_1)_{\alpha_0 \alpha_1} \dots \mathcal{A}^d(x_d)_{\alpha_{d-1} \alpha_d}. \quad (17)$$

4. A weak derivative generalizes the derivative concept for (non)-differentiable functions and is implicitly defined as: e.g. $v \in L^1([a, b])$ is a weak derivative of $u \in L^1([a, b])$ if for all smooth φ with $\varphi(a) = \varphi(b) = 0$: $\int_a^b u(t) \varphi'(t) dt = - \int_a^b v(t) \varphi(t) dt$.

FTT approximation in Eqn 17 projects the target function to a subspace with finite basis. And the approximation error can be bounded using the following Lemma:

Lemma 5 (FTT Approximation Bigoni et al. (2016)) *Let $f \in \mathcal{H}_\mu^k$ be a Hölder continuous function, defined on a bounded domain $\mathbf{I} = I_1 \times \dots \times I_d \subset \mathbb{R}^d$ with exponent $\alpha > 1/2$, the FTT approximation error can be upper bounded as*

$$\|f - f_{TT}\|^2 \leq \|f\|^2 (d-1) \frac{(r+1)^{-(k-1)}}{(k-1)} \quad (18)$$

for $r \geq 1$ and

$$\lim_{r \rightarrow \infty} \|f_{TT} - f\|^2 = 0 \quad (19)$$

for $k > 1$

Lemma 5 relates the approximation error to the dimension d , tensor-train rank r , and the regularity of the target function k . In practice, HOT-RNN implements a polynomial expansion of the input states \mathbf{s} , using powers $[\mathbf{s}, \mathbf{s}^{\otimes 2}, \dots, \mathbf{s}^{\otimes p}]$ to approximate f_{TT} , where p is the degree of the polynomial. We can further use the classic spectral approximation theory to connect the HOT-RNN structure with the degree of the polynomial, i.e., the order of the tensor. Let $I_1 \times \dots \times I_d = \mathbf{I} \subset \mathbb{R}^d$. Given a function f and its polynomial expansion P_{TT} , the approximation error is therefore bounded by:

Lemma 6 (Polynomial Approximation) *Let $f \in \mathcal{H}_\mu^k$ for $k > 0$. Let P be the approximating polynomial with degree p , Then*

$$\|f - P_N f\| \leq C(k) p^{-k} |f|_{k,\mu}$$

Here $|f|_{k,\mu}^2 = \sum_{|i|=k} \|D^{(i)} f\|^2$ is the semi-norm of the space \mathcal{H}_μ^k . $C(k)$ is the coefficient of the spectral expansion. By definition, \mathcal{H}_μ^k is equipped with a norm $\|f\|_{k,\mu}^2 = \sum_{|i| \leq k} \|D^{(i)} f\|^2$ and a semi-norm $|f|_{k,\mu}^2 = \sum_{|i|=k} \|D^{(i)} f\|^2$. For notation simplicity, we muted the subscript μ and used $\|\cdot\|$ for $\|\cdot\|_{L_\mu}$.

So far, we have obtained the tensor-train approximation error with the regularity of the target function f . Next we will connect the tensor-train approximation and the approximation error of neural networks with one layer hidden units. Given a neural network with one hidden layer and sigmoid activation function, following Lemma describes the classic result of describes the error between a target function f and the single hidden-layer neural network that approximates it best:

Lemma 7 (NN Approximation Barron (1993)) *Given a function f with finite Fourier magnitude distribution C_f , there exists a neural network with n hidden units f_n , such that*

$$\|f - f_n\| \leq \frac{C_f}{\sqrt{n}} \quad (20)$$

where $C_f = \int |\omega|_1 |\hat{f}(\omega)| d\omega$ with Fourier representation $f(x) = \int e^{i\omega x} \hat{f}(\omega) d\omega$.

We can now generalize Barron’s approximation lemma 7 to HQT-RNN. The target time series is $f(\mathbf{x}) = f(\mathbf{s} \otimes \cdots \otimes \mathbf{s})$. We can express the function using FTT, followed by the polynomial expansion of the states concatenation P_{TT} . The approximation error of HQT-RNN, viewed as one layer hidden

$$\begin{aligned}
\|f - P_{TT}\| &\leq \|f - f_{TT}\| + \|f_{TT} - P_{TT}\| \\
&\leq \|f\| \sqrt{(d-1) \frac{(r+1)^{-(k-1)}}{(k-1)}} + C(k)p^{-k} |f_{TT}|_k \\
&\leq \|f - f_n\| \sqrt{(d-1) \frac{(r+1)^{-(k-1)}}{(k-1)}} + C(k)p^{-k} \sum_{i=k} \|D^{(i)}(f_{TT} - f_n)\| + o(\|f_n\|) \\
&\leq \frac{C_f^2}{n} \sqrt{(d-1) \frac{(r+1)^{-(k-1)}}{(k-1)}} + C(k)p^{-k} \sum_{i=k} \|D^{(i)} f_{TT}\| + o(\|f_n\|)
\end{aligned}$$

Where p is the order of tensor and r is the tensor-train rank. As the rank of the tensor-train and the polynomial order increase, the required size of the hidden units become smaller, up to a constant that depends on the regularity of the underlying dynamics f .

.2 Additional Experiments

Genz dynamics Genz functions are often used as basis for evaluating high-dimensional function approximation. Figure 14 visualizes different Genz functions, realizations of dynamics and predictions from HQT-LSTM and baselines. We can see for “oscillatory”, “product peak” and “Gaussian”, HQT-LSTM can better capture the complex dynamics, leading to more accurate predictions.

Moving MNIST Moving MNIST Srivastava et al. (2015) generates around 50,000 video sequences of length 100 on the fly. The video is generated by moving the digits in the MNIST image dataset along a given trajectory within a canvas of size 48×48 . The trajectory reflects the dynamics of the movement. In this experiment, we used *cos* and *sin* velocity.

HIGHER-ORDER TENSOR RNNs

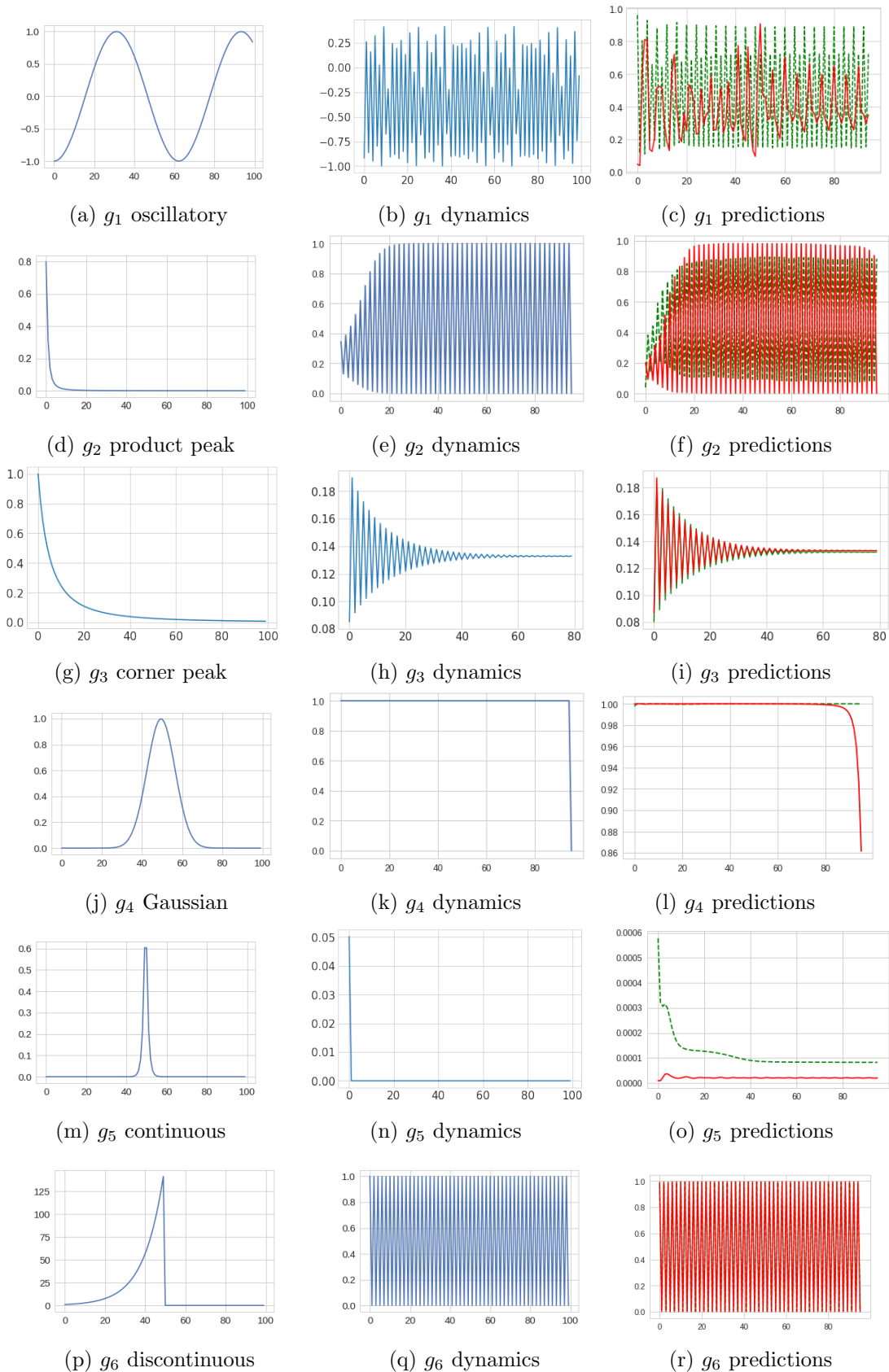


Figure 13: Visualizations of Genz functions, dynamics and predictions from HOT-LSTM and baselines. Left column: transition functions, middle: realization of the dynamics and right: model predictions for LSTM (green) and HOT-LSTM (red).

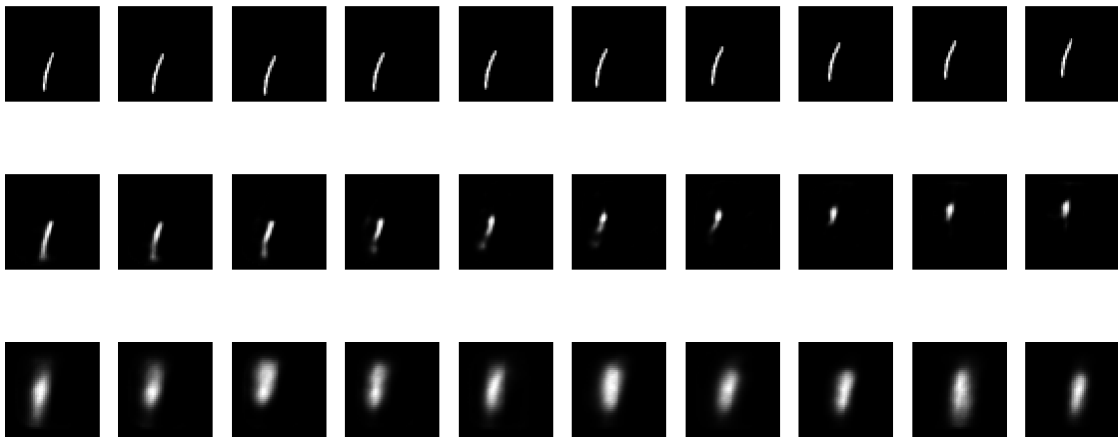


Figure 14: Visualizations of ground truth and predictions from HOT-LSTM and baselines for moving MNIST. Top: ground truth; Middle: LSTM predictions; Bottom: HOT-LSTM predictions.